Quantum-cascade laser integrated with a metal–dielectric–metal-based plasmonic antenna

Dibyendu Dey,[1,*] John Kohoutek,[1] Ryan M. Gelfand,[1] Alireza Bonakdar,[1] and Hooman Mohseni[1,2]

[1]*Department of Electrical Engineering and Computer Science, Northwestern University,*
2145 Sheridan Road, Evanston, Illinois. 60208, USA

[2]*E-mail: hmohseni@ece.northwestern.edu*
*Corresponding author: dey@u.northwestern.edu

Optical nanoantennas are capable of enhancing the near-field intensity and confining optical energy within a small spot size. We report a novel metal–dielectric–metal coupled-nanorods antenna integrated on the facet of a quantum-cascade laser. Finite-difference time-domain simulations showed that, for dielectric thicknesses in the range from 10 to 30 nm, peak optical intensity at the top of the antenna gap is 4000 times greater than the incident field intensity. This is 4 times higher enhancement compared to a coupled metal antenna. The antenna is fabricated using focused ion-beam milling and measured using modified scanning probe microscopy. Such a device has potential applications in building mid-IR biosensors.   © 2010 Optical Society of America

OCIS codes: 140.5965, 250.5403, 280.1415, 240.6680.

At the interface between two mediums having opposing signs of dielectric susceptibility (e.g., metal–dielectric) light can generate a collective motion of conductive electrons, known as surface plasmons (SPs) [1]. The principle of SPs has been extensively applied in many novel applications. including extraordinary optical transmission [2], SP interference lithography [3], biosensing [4], and spectroscopic applications [5].

Currently there is increasing interest in making active plasmonic devices based on quantum-cascade lasers (QCLs) [6,7]—unipolar semiconductor lasers [8,9] that work on the principle of intersubband transitions. This type of laser operates efficiently in the mid-IR region (2–30 μm) of the optical spectrum. Plasmonic QCL devices based on a single metal antenna have been recently demonstrated to enhance the local electromagnetic field [10,11]. Here, we demonstrate a metal–dielectric–metal (MDM)-based coupled-nanorods antenna design that shows considerable improvement in terms of peak intensity enhancement.

To analyze the performance of our MDM antenna, we simulated the structure using commercially available three-dimensional finite-difference time-domain (FDTD) software, Lumerical. All material data used in the simulation, other than the laser region, is from [12]. The refractive index of the laser material is chosen to be 3.2, which is the weighted average of the refractive index of the active region, $In_{0.44}Al_{0.56}As/In_{0.6}Ga_{0.4}As$.

An optical TM-polarized plane wave with lasing wavelength at 5.97 μm (found from the emission spectrum of the device) is used as the source for all performed FDTD simulations. At resonance, the surface charge is accumulated at the end of each nanorod and it is maximized at the gap between two closely placed nanorods due to capacitive coupling [13]. The accumulated charge leads to large electric field intensity enhancement at the vicinity of the gap [14].

To understand the effect of dielectric thickness on intensity enhancement, the SiO_2 thickness of the MDM antenna design has been varied at 0, 10, 20, 30, 50, and 100 nm while keeping the total thickness of the compo-

site MDM layer constant at 170 nm. The simulated peak intensity enhancement at the antenna gap on the same level as the top surface is plotted against varying lengths of the antenna in Fig. 1(a). As the SiO_2 thickness is changed from 10 to 30 nm, there is an approximately fourfold increase in peak optical intensity. The side view of the antenna shows the intensity profile for optimized MDM antenna design [Fig. 1(b)]. The electric field map of the MDM structure [Fig. 2(a)] shows that multiple coupling mechanisms are involved in generating near-field enhancement. At the beginning, the incident laser light generates SPs on the bottom Au/buffer SiO_2 interface. Because of vertical plasmon coupling, surface charges are induced on the top Au and, simultaneously, a strong electric field is generated inside the sandwiched dielectric. From Fig. 2(a), it can also be found that most of the electromagnetic field resides inside the sandwiched
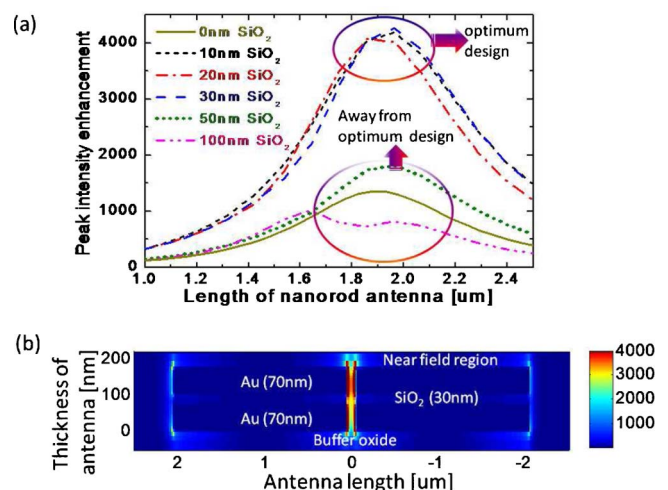

Fig. 1.   (Color online) (a) Plot shows the peak intensity enhancement versus antenna length. The silicon dioxide thickness for the MDM structure has been varied at 0, 10, 20, 30, 50, and 100 nm while keeping the total thickness of the structure constant at 170 nm. (b) Side view of the simulated intensity profile for the MDM antenna ($Au/SiO_2/Au$, 70/30/70 nm) at resonance antenna length of 2 μm.

dielectric, and thus there is little absorption loss due to the metal. Finally, the induced dipole moments at each vertically coupled Au antenna couple radiatively to generate strong near-field enhancement. Increasing the sandwiched dielectric thickness beyond 30 nm affects the vertical coupling efficiency negatively.

After optimizing our design, we experimentally measured the electric field enhancement. We fabricated a QCL with a nanopatterned antenna on the facet and used an apertureless near-field scanning optical microscope (NSOM) to probe it. Our QCL is based on $In_{0.44}Al_{0.56}As/In_{0.6}Ga_{0.4}As$, with a core design as outlined in a previous paper [15]. After cleaving, the lasers were mounted on a c-mount and tested for current-voltage performance at room temperature. After initial characterization, one facet of the device was coated with $SiO_2/Au/SiO_2/Au$ (100/70 nm/30 nm/70 nm) by electron-beam evaporation.

The nanorod antenna was then fabricated on the coated facet of the laser using a focused ion beam (Hellios FEI). Using the gallium ion beam at high voltage (30 keV) and low current (48 pA), a high precision of milling was achieved. The fabricated antenna on the facet of QCL is shown in the inset of Fig. 2(a). Figure 2(b) shows a magnified scanning electron microscope (SEM) image of the coupled antenna. The threshold current of the laser at room temperature, operating in pulsed mode with 1% duty cycle (100 ns, 100 KHz), was found to be 2.28 and 1.68 A, respectively, with and without fabricated antenna. The reduction in threshold current is due to increasing reflectivity from the facet by the metal coating. The near-field images and topography of the patterned QCL were then simultaneously measured with a custom-designed mid-IR
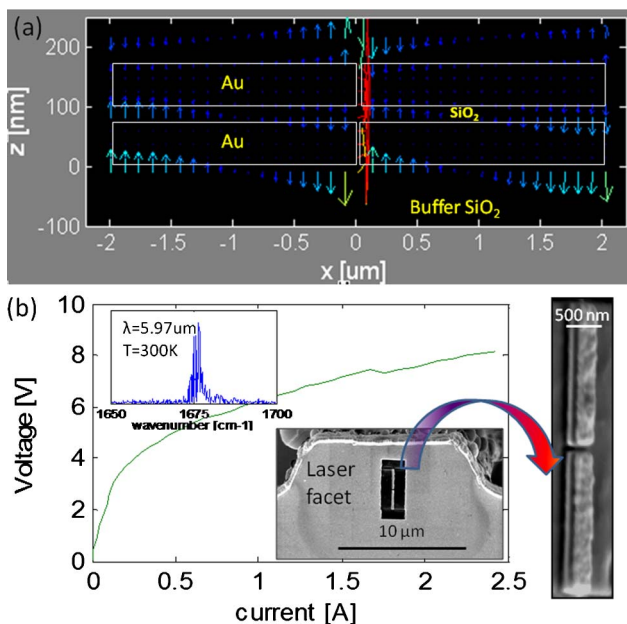

Fig. 2. (Color online) (a) Electric field distribution along the xz plane for the MDM antenna at $y = 0$. (b) Current–voltage characteristics of QCL integrated with a coupled nanorods antenna. Top left inset, emission spectrum at 300 K for a QCL with an integrated antenna. Bottom right inset, SEM image of the $Au/SiO_2/Au$ (70/30/70 nm) coupled-nanorods antenna integrated on the facet of a QCL. A magnified SEM image is shown on the right-hand side.

NSOM [16]. Commercially available NSOMs generally use a spatially confined optical spot at the end of a hollow metallic scanning tip to selectively illuminate the probed surface and produce an image beyond the diffraction limit. However, this setup involves complicated intermediate optics and an external light source. In contrast, we have built a mid-IR NSOM (Fig. 3) based on a commercially available atomic force microscope (AFM) (Agilent 5400). During measurement, the apex of the AFM tip was used to scatter the near-field intensity from the antenna structure. The scattered beam was collimated by an objective lens and then collected using a mercury–cadmium–telluride detector. A lock-in detection technique at the tapping frequency was then utilized to filter the scattered signal from the background noise generated due to scattering from the surface of the cantilever.

There are two components of scattered electric field, E_x (in-plane) and E_z (out-of-plane), interacting with the oscillating AFM tip, and only the significant component of the near field is expected to be recorded. The electric field components on the plane of the sample surface yield a relatively weak scattering signal compared to the component perpendicular to it (E_z) [17,18]. Thus, our NSOM measures E_z components of the field [19]. In Figs. 4(c) and 4(d), the topography and NSOM image of $Au/SiO_2/Au$ (70/30/70 nm) coupled nanorods antenna are shown, where the resonant length of antenna is 2.0 μm. The FWHM of the center spot has been found to be ~450 nm. Away from the resonance length, the optical hot spot has not been found, as seen from the topographic and NSOM measurement of coupled nanorods at an antenna length of 1.5 μm [Figs. 4(e) and 4(f)]. In Figs. 4(a) and 4(b), a simulated E_z field is shown for resonant and off-resonant antennas. The experimentally measured NSOM image matches closely with the simulated E_z component of the resonant antenna. Although the simulation showed maximum field intensity at both ends of the coupled antenna, experimentally measured NSOM data repeatedly showed two bright spots. At this point, we believe it is due to the hybridization of the symmetric and antisymmetric modes of the coupled antenna, as discussed in [20]. We plan to further investigate it in the near future.

The near-field images of the antenna were recorded with high pixel resolution and with a reduced scan speed
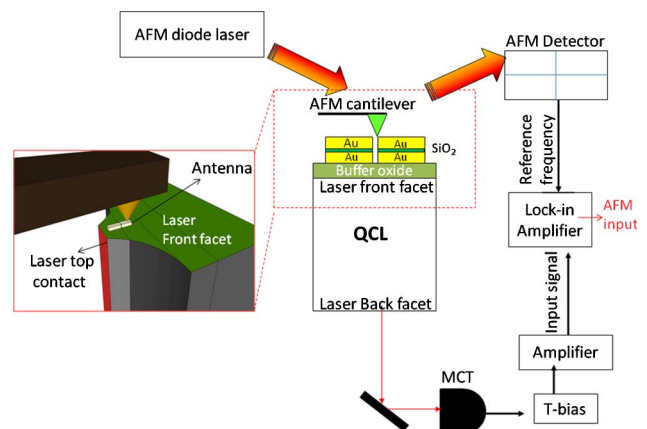

Fig. 3. (Color online) Schematic diagram showing the NSOM setup for simultaneous measurement of the topography and near-field intensity of the MDM antenna integrated with a QCL.
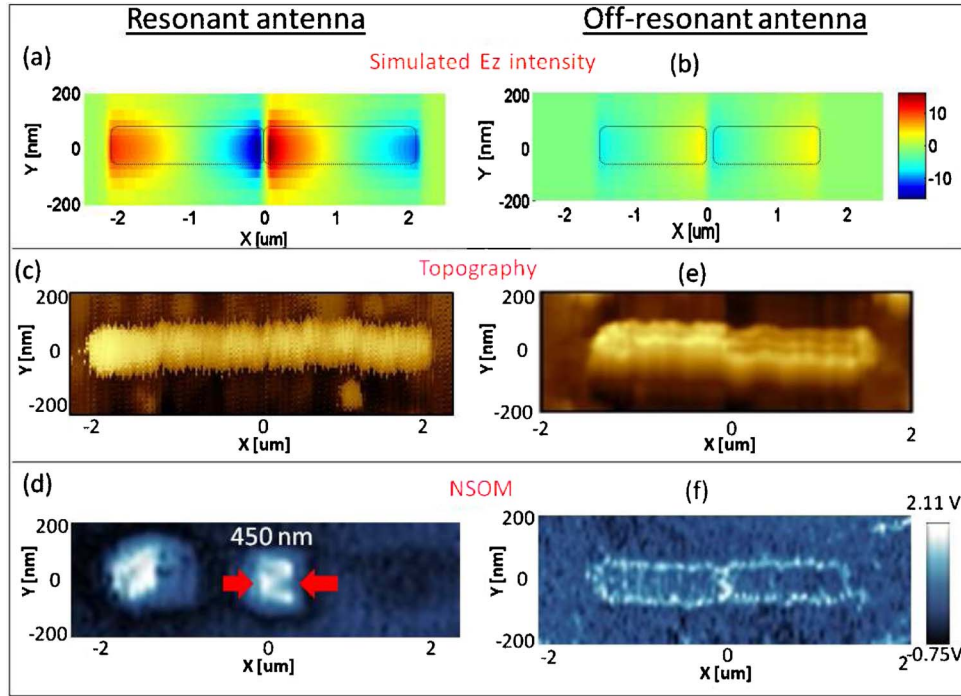
Fig. 4.   (Color online) (a), (b) Top views of simulated E_z field along the antenna axis, 50 nm above the top metal surface, for resonant antenna (length of antenna $= 2 \, \mu$m) and nonresonant antenna (length of antenna $a = 1.5 \, \mu$m). (c), (d) Topography and NSOM image of the Au/SiO$_2$/Au (70/30/70 nm) resonant coupled nanorods integrated on the facet of a QCL. (e), (f) Topography and NSOM image of the Au/SiO$_2$/Au (70/30/70 nm) off-resonant coupled nanorods integrated on the facet of the QCL. Here x and y represent the length and the width of the antenna, respectively.

of 0.1 lines/s. The image distortions, as seen in Figs. 4(c) and 4(e), are due to small drifts in sample position occurring over the long acquisition time for NSOM measurement. During the NSOM measurement, the laser was operated at 1% duty cycle near the threshold voltage with an average power output of 100 μW. Based on our simulation, the average intensity enhancement can be up to a factor of 4000 and thus, by neglecting any incurred optical losses, there can be high power density inside the "hot spot" region.

In conclusion, we have demonstrated NSOM of an MDM coupled-nanorods antenna integrated on to the facet of a QCL. FDTD simulation results were used to optimize the dielectric thickness in the range from 10 to 30 nm. These simulations also indicate that, at resonance, the peak intensity from the antenna can be up to 4000 times the incident field intensity. This is a fourfold improvement over the single metal design. Experimental results with the MDM antenna have the ability to confine the lasing mode to a spot size as small as ~450 nm, which is more than 10 times smaller than the wavelength of the laser. The experimental results of laser confinement were further validated using finite element modeling. Such high intensity, hot spot locations can be used in increasing photon interaction with biomolecules for sensing applications [21].

References

1. H. Raether, *Surface Plasmons on Smooth and Rough Surfaces and on Gratings* (Springer-Verlag, 1998).
2. T. W. Ebbesen, H. J. Lezec, H. F. Ghaemi, T. Thio, and P. A. Wolff, Nature **391**, 667 (1998).
3. Z. Liu, J. M. Steele, W. Srituravanich, Y. Pikus, C. Sun, and X. Zhang, Nano Lett. **5**, 1726 (2005).
4. J. N. Farahani, D. W. Pohl, H.-J. Eisler, and B. Hecht, Phys. Rev. Lett. **95**, 017402 (2005).
5. S. Nie and S. R. Emory, Science **275**, 1102 (1997).
6. N. Yu, J. Fan, Q. J. Wang, C. Pflugl, L. Diehl, T. Edamura, M. Yamanishi, H. Kan, and F. Capasso, Nat. Photon. **2**, 564 (2008).
7. N. Yu, E. Cubukcu, L. Diehl, D. Bourm, S. Corzine, J. Zhu, G. Hofler, K. B. Crozier, and F. Capasso, Opt. Express **15**, 13272 (2007).
8. J. Faist, F. Capasso, D. L. Sivco, C. Sirtori, A. L. Hutchinson, and A. Y. Cho, Science **264**, 553 (1994).
9. Y. Bai, S. Slivken, S. Kuboya, S. R. Darvish, and M. Razeghi, Nat. Photon. **4**, 99 (2010).
10. E. Cubukcu, N. Yu, E. J. Smythe, L. Diehl, K. B. Crozier, and F. Capasso, IEEE J. Sel. Top. Quantum Electron. **14**, 1448 (2008).
11. E. Cubukcu, E. A. Kort, K. B. Crozier, and F. Capasso, Appl. Phys. Lett. **89**, 093120 (2006).
12. D. Palik, *Handbook of Optical Constants of Solids*, Vol. 1 (Academic 1985).
13. N. Yu, E. Cubukcu, L. Diehl, M. A. Belkin, K. B. Crozier, and F. Capasso, Appl. Phys. Lett. **91**, 173113 (2007).
14. J. Aizupura, G. W. Bryant, L. J. Ritcher, F. J. G. De Abajo, B. K. Kelley, and T. Mallouk, Phys. Rev. B **71**, 235420 (2005).
15. L. Diehl, D. Bour, S. Corzine, J. Zhu, G. Hofler, M. Loncar, M. Troccoli, and F. Capasso, Appl. Phys. Lett. **89**, 081101 (2006).
16. B. Hecht, H. Bielefeldt, Y. Inouye, D. W. Pohl, and L. Novotny, J. Appl. Phys. **81**, 2492 (1997).
17. M. Knoll and F. Keilmann, Opt. Commun. **182**, 321 (2000).
18. R. Hillenbrand, B. Knoll, and F. Keilmann, J. Microsc. **202**, 77 (2001).
19. R. L. Olmon, P. M. Krentz, A. C. Jones, G. D. Boreman, and M. B. Raschke, Opt. Express **16**, 20295 (2008).
20. L. Wang, J. Zhang, X. Wu, J. Yang, and Q. Gong, Opt. Commun. **281**, 5444 (2008).
21. M. F. Garcia-Parajo, Nat. Photonics **2**, 201 (2008).